IN VIVO CHARACTERIZATION OF A PREVASCULARIZED, LOAD-BEARING SCAFFOLD FOR BONE REGENERATION

By

CHRISTIAN E. BUCKLEY

A thesis submitted to the

School of Graduate Studies

Rutgers, The State University of New Jersey

In partial fulfillment of the requirements of

Master of Science

Graduate program in Biomedical Engineering

Written under the direction of

Joseph W. Freeman

And approved by

_____

_____

_____

New Brunswick, New Jersey

October, 2019

ABSTRACT OF THE THESIS

In Vivo Characterization of a Prevascularized, Load-Bearing Scaffold for Bone Regeneration

By CHRISTIAN E. BUCKLEY

Thesis Director:

Dr. Joseph W. Freeman

Due to the increasing number of orthopedic injuries occurring each year, there is a critical need for better treatments of improperly healed fractures. Today's treatments, such as autografts, allografts, and biocompatible ceramics, all have their own drawbacks, including donor site morbidity, disease transmission, and poor degradation rates. To circumvent these problems, bone tissue engineering utilizes various biocompatible materials and cells to mimic native bone while new tissue is created. We have developed a prevascularized tissue-engineered scaffold that combines two stereoisomers of polylactic acid and hydroxyapatite to simultaneously entice osteogenic and vascular differentiation of mesenchymal stem cells. In this study, we have implanted these scaffolds into a radial defect model in New Zealand white rabbits for 8 weeks. Radiographic images at 4 and 8 weeks have shown considerable remodeling occurring at the implant site and stable implants throughout the study. Results from micro computed

tomography showed a large amount of new bone growth into and around the scaffold, both quantitatively and qualitatively. Mechanical testing resulted in similar amounts of force required to remove the scaffold from the implant site when compared to the allograft control. Finally, histological analysis showed collagen deposition into and around the scaffolds with many cells present throughout. Signs of vasculature can be seen in the osteons but there is little evidence of angiogenesis. The tissue-engineered scaffold used in this study was comparable to an allograft, one of today's gold standards, and shows potential to be a clinically useful alternative.

Acknowledgements

I would like to start off by thanking the rabbits that were used throughout this study. You gave the ultimate sacrifice and will not be forgotten.

There are an incredible amount of people that have helped me in one way or another throughout the duration of my Masters studies. Thank you to Dr. Charlie Gatt, Barbara Perry, William Pfaff, and all of the vets and vet techs who helped with the rabbit study. You were all so incredibly helpful even when things did not go as planned. Patricia Buckendahl was an enormous help running Micro CT on the implants and creating beautiful GIFs that gave me my first real taste of exciting data. Thank you to Mike Pellegrini for teaching me literally every single skill that I have learned as a biomedical engineer. Without you I wouldn't even be able to culture a cell without killing it. A very special thanks to Dr. Joseph Freeman for the invaluable guidance he has given me over the past three years. He was instrumental in shaping me into the scientist that I am today and I will continue to apply what he has taught me throughout all of my future studies. I am forever grateful for all of the opportunities he has given me and especially for all of the lab lunches at Jose Tejas and Red Robin. Finally, thank you to everyone who I have had the pleasure of spending time with in and out of the lab, especially Bobby, Mike, Fernando, Tim, Linh, Mary Pat, and Alex. You guys saved me from many one-sided conversations with my cells and my rabbits.

Most importantly, thank you to all my family and friends who have supported me throughout this hectic journey. Thank you to my parents for showing me how to live as a decent human being and how to approach problems with both logic and creativity. I could write an entire thesis solely on how much I appreciate what you have done for me. My

siblings, Ryan, Caitlyn, and Alyssa for showing me how to live life to the fullest and paving the way for me so I didn't get yelled at as much by Mom and Dad. Finally, thank you to my amazing girlfriend Rachel. The amount of patience you've shown me over the past five years is truly astounding. Thank you for getting me out of my own head when I needed it most and motivating me to be the best man I can be. I'm incredibly lucky to have people like you in my life and I love you all.

This is just the beginning.

Table of Contents

ABSTRACT OF THE THESIS ii
Acknowledgements iv
LIST OF FIGURES vii
Chapter 1 – Introduction 1
Chapter 2 – Scaffold Fabrication and *In Vivo* Study 7
2.1. Materials and Methods 7
2.1.1. Electrospinning 7
2.1.2. Cortical/Trabecular Assembly 8
2.1.3. Hydroxyapatite Columns 9
2.1.4. Scaffold Assembly 10
2.1.5. Mineralization 11
2.1.6. Vascularization 12
2.1.7. rbMSC Seeding 12
2.1.8. Surgical Procedure 13
2.1.9. Allograft Preparation 13
2.1.10. Micro CT 14
2.1.11. Mechanical Testing 15
2.1.12. Histology 16
2.1.13. Statistical Analysis 18
2.2. Results 18
2.2.1. Radiographic Images 18
2.2.2. Micro CT 19
2.2.3. Mechanical Testing 21
2.2.4. Histology 22
2.3. Discussion 28
Chapter 3 – Conclusions and Future Directions 33
References 35

LIST OF FIGURES

Figure 1: Schematic of Various Approaches to Tissue Engineering..... 4

Figure 2: Schematic of the Electrospinning Process..... 5

Figure 3: Electrospun Cortical and Trabecular Structures..... 9

Figure 4: Sintered Hydroxyapatite Column..... 10

Figure 5: Completed Scaffold..... 11

Figure 6: Scaffold Before and After Implantation..... 15

Figure 7: Experimental Setup for Mechanical Push-Out Test..... 16

Figure 8: Radiographic Images of Implanted Allograft and Scaffold at 4 and 8 Weeks 20

Figure 9: Micro CT Images of Harvested Allograft and Scaffold..... 21

Figure 10: Average Volume of New Bone Growth..... 22

Figure 11: Mechanical Push-Out Test..... 23

Figure 12: Histological Images of the Allograft Sectioned at the End..... 25

Figure 13: Histological Images of the Allograft Sectioned at the Middle..... 26

Figure 14: Histological Images of the Scaffold Sectioned at the End..... 27

Figure 15: Histological Images of the Scaffold Sectioned at the Middle..... 28

Chapter 1 – Introduction

Orthopedic injuries are among some of the leading causes for mortality, morbidity, and hospitalization in both developed and developing countries (1). While the more severe cases that involve multiple fracture sites and soft tissue injuries are generally caused by high energy trauma, fractures can also occur due to minor accidents such as falls. This is especially prevalent in the growing elderly population that is currently experiencing an increase in age-related fractures due to diseases such as osteoporosis (2).

Bone tissue can be divided into two primary types: dense cortical bone and spongy trabecular bone. Highly organized collagen fibrils, mainly type I collagen, are the primary component of both types of bone. These fibrils are interconnected and strengthened by calcium phosphate nanoparticles (3). Cortical bone is the dense outer layer that is important for mechanical support and is also home to osteons and the haversian canal, where the blood vessels and neurons are located. Trabecular bone is less dense and is much more metabolically active, seeing as it is the location of hematopoiesis in humans. As an organ, bone is responsible for calcium homeostasis, provides mechanical support for soft tissues, and acts as a lever for muscle action (4). For these reasons, it is essential that bone tissue functions normally throughout the body.

When a fracture occurs, the body's natural healing response is initiated and various cells are recruited to begin remodeling the site of injury. These cells include mesenchymal stem cells, osteoblasts, osteoclasts, and chondrocytes (5). This process tends to be incredibly reliable and effective; however, it can have disastrous effects when it fails to successfully heal the tissue. Of the 5.6 million fractures that occur in the United

States each year, it is estimated that 5-10% of patients will require additional surgery to correct for improper healing (6). Given that the risk of experiencing a traumatic fracture throughout the lifetime of both males and females is roughly 50%, there is a critical need for better treatment (7).

When surgical intervention is needed to correct improper healing, bone grafts are often used in the process. Bone grafts are generally derived from autologous tissue, allogeneic tissue, or ceramic materials. Autologous bone grafts are composed of bone that has been harvested from the patient's own body, often taken from the iliac crest, and have excellent compatibility with a very low chance of infection. However, the amount of material available for an autograft is severely limited and there is a potential for donor-site morbidity (8). Allografts are samples of bone that have been harvested from a donor, generally a cadaver. After terminal sterilization, allografts have been shown to be effective bone grafts with limited osteoinductive capabilities and are much more available when compared to autografts. However, there is a much higher chance for disease transmission (9). Despite some of its drawbacks, allografts are still one of the favored choices for bone grafts. The incorporation of ceramic materials has become very common for certain grafts as well. These materials tend to have a wide range of properties and can be bioinert, bioactive, or bioresorbable (10). One of the primary ceramics that is used is hydroxyapatite due to the fact that it is naturally found in bone tissue and has favorable mechanical and osteoinductive properties (11). Despite these benefits, ceramics tend to resorb very slowly and are difficult to handle in a clinically-relevant manner.

To alleviate many of the drawbacks associated with autografts, allografts, and biocompatible ceramics, many researchers have begun to explore the field of tissue engineering to restore bone. Tissue engineering combines the practices of biology, materials science, and engineering to modulate and regenerate various cells and tissues throughout the body (Figure 1). By providing cells with the appropriate physical and/or chemical cues, the function of tissues and organs can be restored or improved (12). To date, clinical success has been shown with regenerating flat organs such as skin and cartilage and tubular structures such as blood vessels and tracheas (13, 14, 15). Solid, more complex organs, such as the heart and kidneys, are much more difficult to engineer. The field has seen many incredible advances within the recent decades and there is still an enormous amount of untapped potential waiting to be fostered.

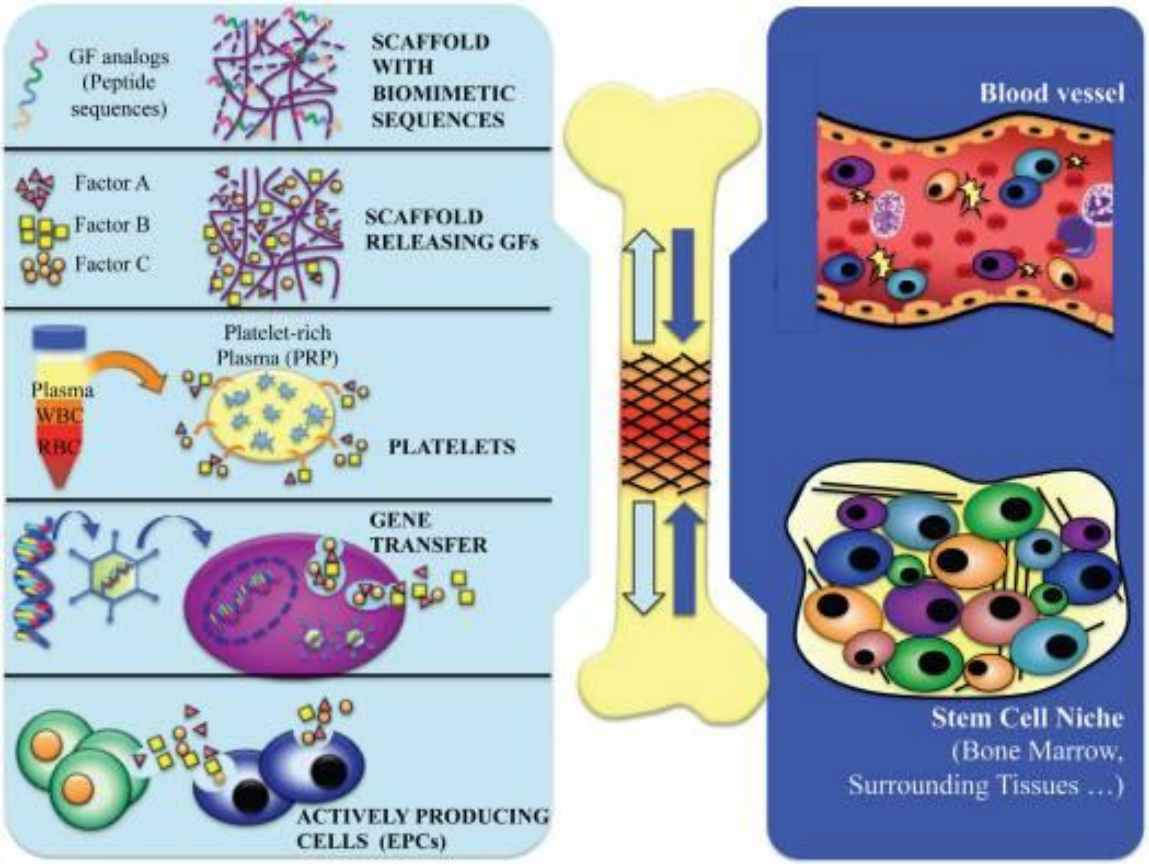

Figure 1. Schematic of various approaches for tissue engineering. Implanted materials and growth factors provide cues for the host tissue to infiltrate and begin to regenerate the tissue at the implant site (16).

In addition to the previously mentioned focuses of tissue engineering, bone tissue engineering has made significant progress in the nearly three decades since it has been established. Researchers have utilized numerous materials to achieve adequate bone regeneration such as polylactic acid (PLA), polylactic-co-glycolic acid (PLGA), polycaprolactone (PCL), and many others. A common method used for fabricating these polymers is electrospinning. Electrospinning is a technique that uses electrostatic forces to weave polymer solutions into nanofibrous sheets (Figure 2). These electrospun sheets have been shown to mimic the microstructural features of native tissues and can help guide cell growth and migration (16). In addition to synthetic polymers, ceramics and advanced hydrogels are being combined to provide the scaffold needed for cells to grow

and differentiate accordingly (17). Scientists have successfully shown new bone growth both *in vitro* and *in vivo* using a wide variety of different materials with the capability to support natural loads (18, 19).

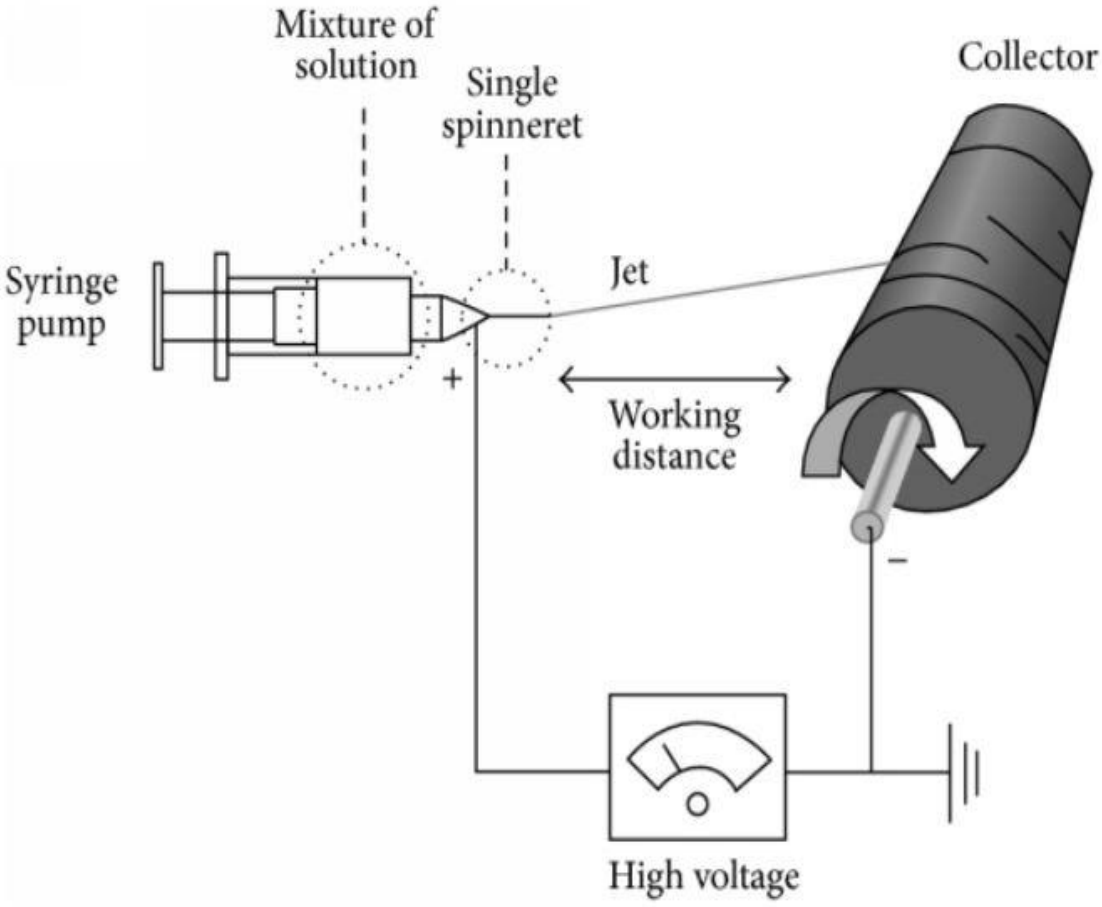

Figure 2. Schematic of the electrospinning process. A solution is pushed through a charged needle and an electrostatic field causes the solution to flow onto a collector. The rotating collector creates a nanofibrous sheet of spun fibers (20).

One of the biggest hurdles to developing functional tissue engineered bone scaffolds has been the inability to introduce vascularization. Vascularization of tissue engineered constructs is critical for the successful integration of the implants into the surrounding tissue and is necessary to support the growing cells throughout the entire scaffold. In order to increase the amount of vascularization that occurs within these

scaffolds, scientists generally utilize two main approaches: the first being a cell-based approach and the second using biomaterials with manufactured microchannel networks (21). Cell-based approaches involve the naturally occurring extracellular matrix (ECM) and microenvironment produced by cells. Endothelial cells are commonly used to create a vascular network in tissue engineered constructs which results in better vascularization when implanted *in vivo*. The materials-based approach promotes vascularization by manufacturing these microchannel vascular networks in the scaffolds themselves to help guide the networks as the cells grow. This can be accomplished by techniques such as soft lithography, photo-patterning, and 3D printing.

To address these unmet clinical needs, we have developed a tissue-engineered scaffold that combines biodegradable polymers, bioceramics, and a cell-based prevascularized lumen in order to regenerate new bone and vascular tissue. In this study, the scaffold is evaluated in a load-bearing *in vivo* model. The scaffold's ability to withstand natural loading, regenerate bone, and develop vascularization *in vivo* is studied.

Chapter 2 – Scaffold Fabrication and *In Vivo* Study

2.1. Materials and Methods

2.1.1. Electrospinning

In order to accurately mimic the various structures of bone tissue, nanofibrous sheets of polylactic acid (PLA) were electrospun and assembled accordingly. PLA was used as the base material for this scaffold due to its favorable biological and mechanical properties (22). Two stereoisomers of PLA, poly-l-lactic acid (PLLA) and Poly-d-lactic acid (PDLA) were used in this study. PLLA was chosen to be the main structural component of the scaffold while PDLA was used to adhere the surrounding layers of PLLA together due to its low glass transition temperature (60°C). A 22% (w/v) PDLA solution was made by dissolving PDLA (MW=124,000, Evonik Birmingham Laboratories) in a 3:1 solution of tetrahydrofuran (THF) and dimethylformaldehyde (DMF), respectively. A 7% (w/v) PLLA solution was made by dissolving PLLA (MW=152,000, Sigma Aldrich) in an 11:4:1 solution of dichloromethane (DCM), DMF, and 10% gelatin solution (Type B, Sigma Aldrich). Gelatin was added to the solution to increase the biocompatibility of the scaffold and enhance cell proliferation.

The desired solution was placed in a 5 mL syringe with an 18 gauge needle attached to it. 1 mL of PDLA solution was electrospun on a mandrel rotating at roughly 2000 RPM by applying a voltage gradient of +10 kV/-5 kV at a working distance of 10 cm. 5 mL of PLLA was then electrospun directly onto the previously spun PDLA layer using a voltage gradient of +15 kV/-10 kV at a working distance of 15 cm. Finally, 1 mL of PDLA was spun on top of the PLLA to create an aligned nanofibrous sheet of PDLA-

PLLA-PDLA. This was chosen because of the fact that PDLA solidifies after it is heated to its glass transition temperature of 60°C, thus acting as an adhesive to hold the various forms of PLA together.

A 10% (w/v) Polyethylene oxide (PEO) solution was made by dissolving PEO (Sigma Aldrich) in 90% ethanol. The PEO solution was then electrospun onto a rotating mandrel by applying a voltage gradient of +10 kV/-3 kV at a working distance of 10 cm.

2.1.2. Cortical/Trabecular Assembly

To mimic the cortical section of bone, a thin sheet of electrospun PEO was first tightly wrapped around a 22 gauge needle. The PDLA/PLLA sheet was cut into thin sheets at 45º to mimic the orientation of collagen fibers in natural bone. These strips were wrapped tightly around the PEO and subsequently sintered at 60°C for 45 minutes to sinter the PDLA and create a solid cylinder. The PEO layer was then leached away by soaking the cylinders in deionized (DI) water for 30 minutes and the cylinders were removed from the needles. By leaching away the PEO layer, the inner portion of the PDLA/PLLA cylinder was not damaged during removal. The hardened PDLA/PLLA was created to mimic the cortical portion of bone while the hollow inner channel allowed for inclusion of the haversian canal.

To recreate the porous trabecular section of bone, the same method for electrospinning the cortical bone was used. However, salt was added intermittently onto the nanofibrous sheets as they were being electrospun, allowing salt crystals to be embedded within the sheets throughout the process. At the end of electrospinning, pieces of the sheets were cut into 1.5 cm wide strips and wrapped tightly around a 2.5 cm wide

piece of cardboard and sintered at 60°C for 45 minutes to allow the material to harden. Once sintered, the pieces were submerged in DI water for 30 minutes to leach out the salt crystals that were embedded in the structure, thus resulting in a porous, electrospun material that is similar to trabecular bone. After electrospinning, both the cortical and trabecular pieces were placed in 12% microbial transglutaminase (mTG) for 5 hours at 37°C to crosslink the gelatin (23).

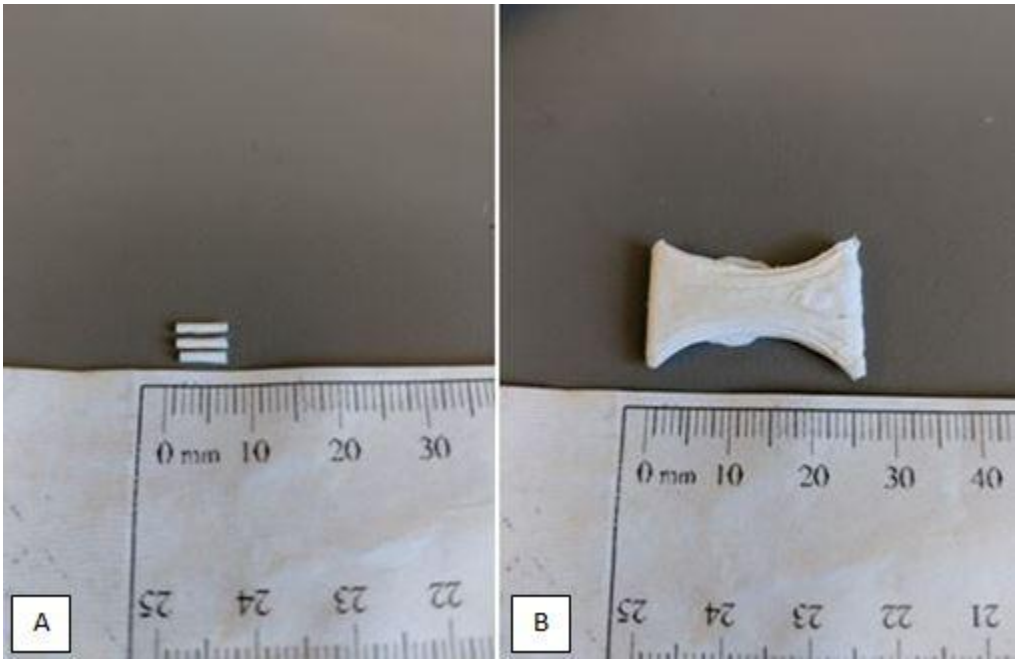

Figure 3. Rolled and sintered PLLA/PDLA osteon structures (A). Sintered and leached PLLA/PDLA trabecular structure (B).

2.1.3. Hydroxyapatite Columns

The final component of the scaffolds was the addition of hydroxyapatite (HAp) columns. As the main inorganic mineral found in bone, these ceramic columns served as structural supports to help the scaffold bear appropriate loads and to provide a more natural biological environment for cells. These HAp columns have also been shown to help with osteogenic differentiation (24). HAp nanopowder (<200 nm particle size,

Sigma Aldrich) was packed tightly into a 1.5x14 mm cylindrical channel and a small amount of water was added intermittently. Once the channel was filled with packed HAp powder, 44 MPa of pressure was applied for 10 minutes using an Instron **(**Model 5869, Norwood, MA). The columns were then carefully removed from the channels and sintered at 1200℃ for 5 hours to harden the ceramic columns.

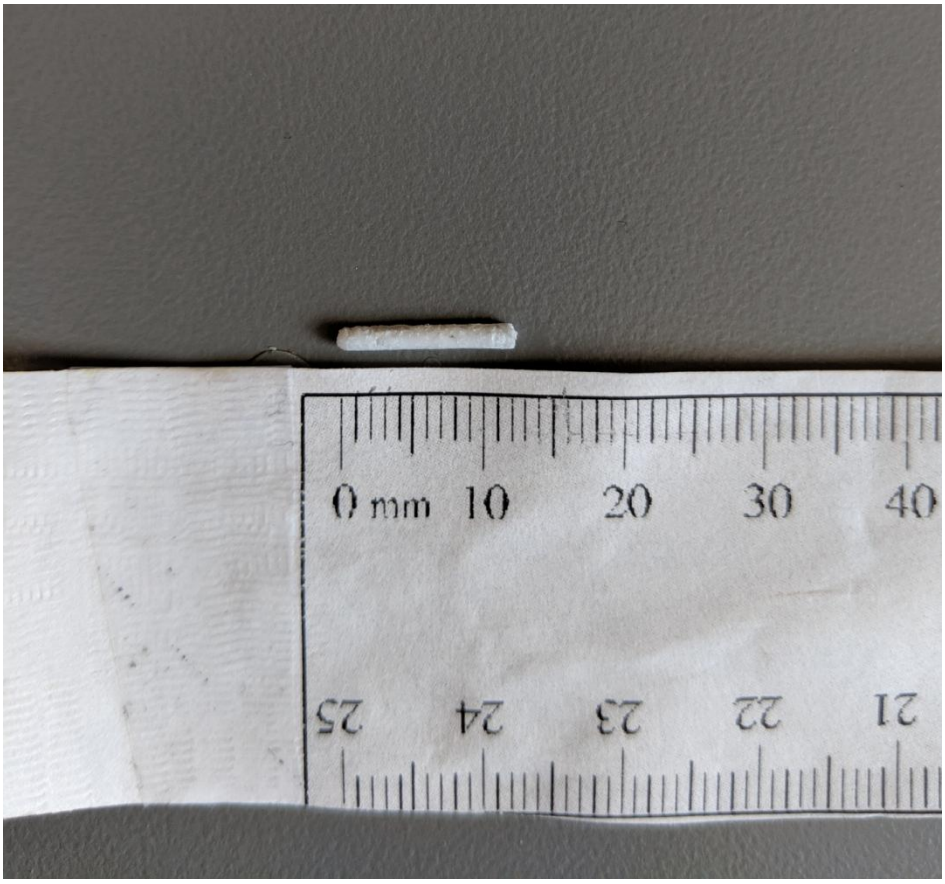

Figure 4. Sintered hydroxyapatite post.

2.1.4. Scaffold Assembly

The HAp columns and osteons were then positioned around the trabecular section and wrapped with a thin sheet of PDLA to hold the structure together. The entire scaffold was then sintered at 60℃ for one hour to allow the surrounding PDLA to harden and create the final stable scaffold (24, Figure 5).

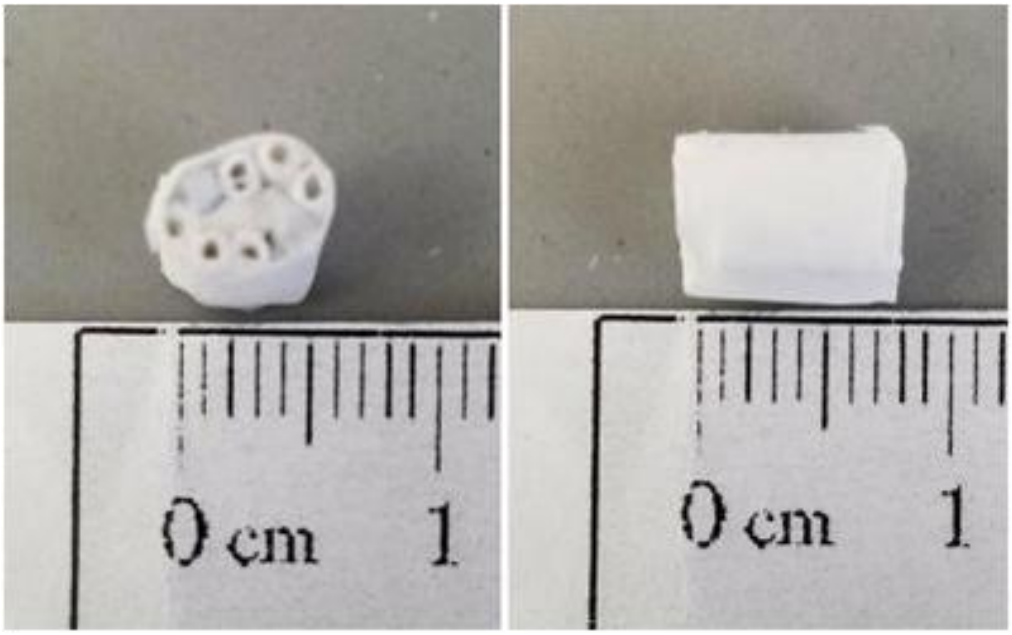

Figure 5. Completed scaffolds. 6 hollow osteons and 2 HAp columns surround pieces of the trabecular portion. The entire scaffold is held together by sintered sheets of PDLA (25).

2.1.5. Mineralization

To help induce osteogenic differentiation of stem cells (25), the completed scaffolds were mineralized using a solution of 10x simulated body fluid (SBF). SBF solution consisted of sodium chloride, potassium chloride, calcium chloride dihydrate, magnesium chloride hexahydrate, sodium phosphate monobasic, and sodium bicarbonate dissolved in DI water. In order to prevent mineralization of the inner portions of the osteons, 8% sodium alginate (FMC BioPolymer) solution was injected directly into the channels and subsequently submerged in a 0.1M calcium chloride solution to crosslink the alginate. Once crosslinked, the scaffolds were placed in a solution of SBF and gently agitated for a total of 10 hours. Throughout the process, fresh SBF solution was added every 2 hours to allow for complete mineralization. After 10 hours, the scaffolds were submerged in phosphate-buffered saline (PBS) to help uncrosslink the alginate, which was then physically removed from the osteons using a blunt needle.

2.1.6. Vascularization

In order to induce vascular differentiation of stem cells (25), the inner portions of the osteons were prevascularized using human dermal microvascular endothelial cells (HMEC-1, ATCC). HMEC-1s were cultured on tissue culture polystyrene (TCP) in MDCB-31 media (Gibco) supplemented with 10% fetal bovine serum (FBS), 1% Penicillin/Streptomycin, 10 mM L-Glutamine, 1 µg/ml Hydrocortisone, and 10 ng/ml Human Epidermal Growth Factor. Cells were grown in a sterile incubator at 37℃ and 5% CO_2. Upon reaching roughly 80% confluency, cells were detached using TrypLE Express Reagent and were seeded inside the osteon channels at a density of 50,000 cells/cm^2. The HMEC-1s were allowed to grow inside the osteons for a period of 14 days, with fresh media being added every 2 to 3 days.

After 14 days, the scaffolds were decellularized using a freeze-thaw method to remove the cells while preserving the extracellular matrix (26). Scaffolds were placed at -80℃ for 30 minutes and then immediately placed in a 37℃ water bath to lyse the cells. After 10 minutes, the scaffolds were rinsed with sterile PBS and the process was repeated for a total of 3 cycles for full decellularization.

2.1.7. rbMSC Seeding

Rabbit Mesenchymal Stromal Cells (rbMSCs, Cyagen) were cultured on TCP in rbMSC media (Gibco) supplemented with 10% FBS, 1% Penicillin/Streptomycin, and 1% L-Glutamine. The cells were allowed to reach roughly 80% confluency and were subsequently detached using TrypLE Express Reagent. 24 hours prior to implantation, 3 to 5 million rbMSCs were seeded inside of the osteon channels and in the trabecular sections of each scaffold.

2.1.8. Surgical Procedure

In order to test the efficacy of the scaffolds in a load-bearing environment, prevascularized, mineralized scaffolds were implanted in adult female New Zealand white rabbits obtained from Charles River Laboratories and Robinson Services Inc. Rabbits were anesthetized and a radial defect was created by removing a piece of the radius that matched the size of the implant (Figure 6A). The scaffolds were implanted into the defect and secured using a 2-0 Ethibond suture (Ethicon). After wound closure, a cast was made around the surgical arm of the rabbits to ensure the stability of the scaffolds. Proper application of the cast proved to be critical in the first 4 weeks to stabilize the surgical leg and ensure the rabbits did not damage the implants. The rabbits were allowed to roam freely in cages and apply pressure on the cast for 4 weeks before the cast was removed. After cast removal, the implants were kept inside the rabbits for an additional 4 weeks. After 8 weeks of implantation, the rabbits were sacrificed and the implants were harvested along with the surrounding radius and ulna. Radiographic images were taken using a Gierth RHF 200 ML X-Ray machine (44 KVp and 5mAs) with dicomPACS DX-R Version 6.0.42-1895 software at weeks 4 and 8 to confirm that the implants were intact and there was no damage to any of the surrounding anatomy.

2.1.9. Allograft Preparation

After 8 weeks, the non-surgical radius was removed in order to procure bone to be used as an allograft control for the study. Allografts were prepared by cutting the radius into 8mm sections and scraping away any excess tissue surrounding the bone. The inner section of the bone was thoroughly rinsed with PBS. After cleaning the sections, the

allografts were exposed to ethylene oxide gas to completely sterilize the samples (27). After sterilization, allografts were implanted in New Zealand White Rabbits using the same method as the experimental scaffolds.

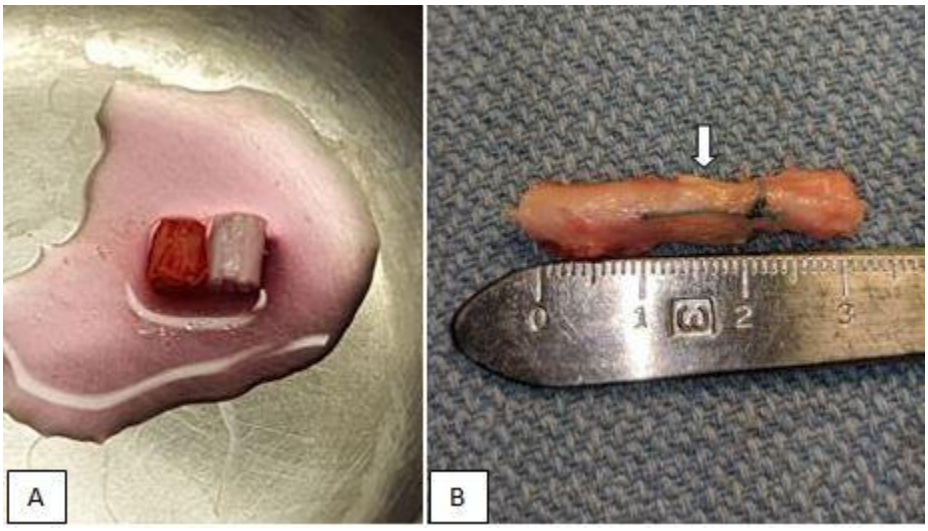

Figure 6. Size comparison of the excised radial segment (left) and the scaffold to be implanted (right) (A). Harvested implant (arrow) with native radius on each side. The scaffold is secured with a suture (blue) (B).

2.1.10. Micro CT

Harvested scaffolds were prepared for micro computed tomography (Micro CT) by removing most of the remaining native bone and surrounding tissue and soaking in isotonic saline for one day. Samples were scanned using the Bruker Skyscan 1272 (90 kV, 111 µA, 1.5 k camera, 8.5 µm pixel size, and a rotation step of 0.4 degrees). Vivoquant software was used to segment the various components of the scaffold based on differences in attenuation. A sample size of 4 was used for each group.

2.1.11. Mechanical Testing

In order to indirectly test the amount of fusion with the surrounding native bone, a mechanical push-out test was performed on the implants. The connected ulnas were carefully cut axially next to each insertion point to ensure the movement of the implants was not restrained by the ulna. Samples were hydrated in PBS for 30 minutes to 1 hour and then secured at each end by vises placed directly under an Instron. The suture in each sample was also cut before testing. Metal bars were customized to fit the radius and length of the implants and were secured to the Instron using pneumatic grips. These bars applied a perpendicular force to the implants at a rate of 1 mm/min until the implants were dislodged from the radius. The ultimate stress was recorded to compare the amount of fusion between groups. A sample size of 4 was used for each group.

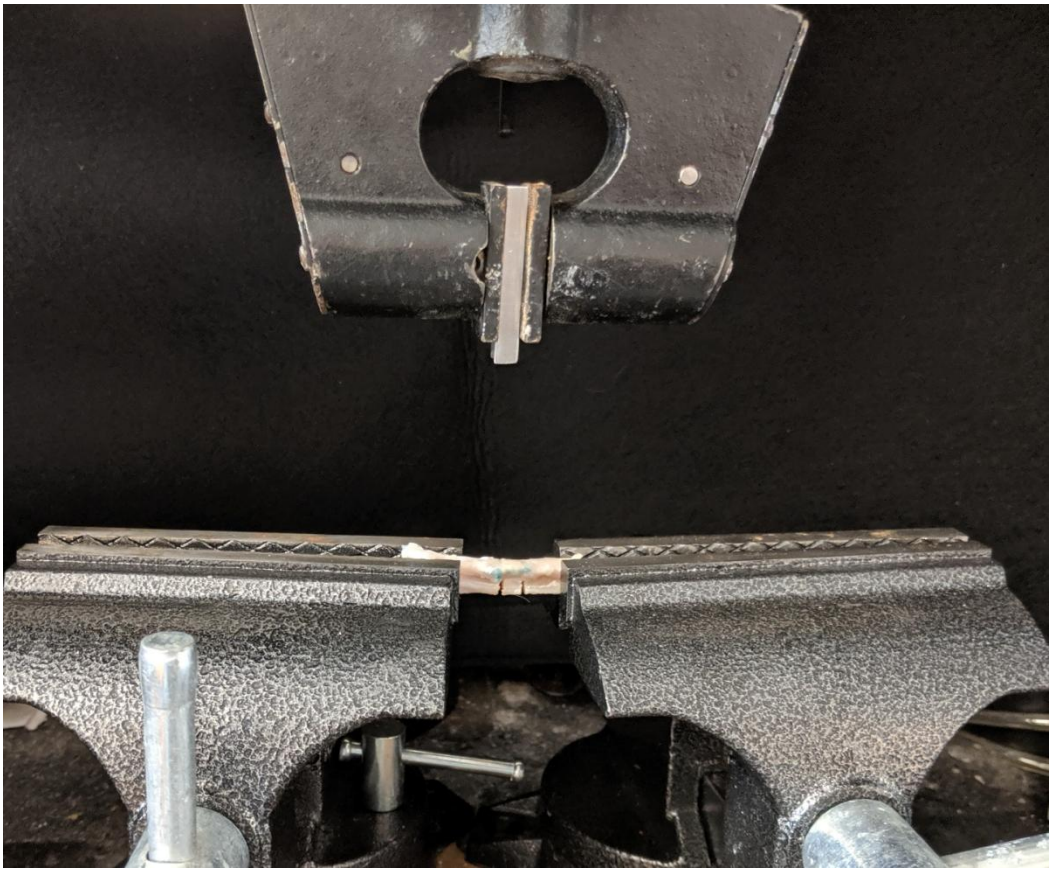

Figure 7. Experimental setup for the mechanical push-out test. The scaffold was secured between two vises and the customized metal bar was secured using pneumatic grips. The adjacent ulna was cut at each insertion point of the scaffold and force was applied perpendicular to the scaffolds.

2.1.12. Histology

To prepare the harvested implants for histology, samples from each group were fixed in 10% neutral buffered formalin for 48 hours and then placed in 10% EDTA solution and gently agitated for 25 days to allow for decalcification. The solution was changed every 2 to 3 days and decalcification was complete when two successive chemical endpoint tests were positive. Fresh decalcification fluid was allowed to soak the implants for roughly one hour. 5 mL of used solution was then taken from the sample and was brought to a pH between 3.2 and 3.6 to dissociate any chelated calcium ions from the EDTA. 5 mL of 3% ammonium oxalate solution was added and allowed to sit for roughly 30 minutes. If calcium is present in the decalcification solution, a precipitate will form

and the solution will become cloudy or turbid. If no precipitate forms, there is no calcium present in the solution. After the first successful test with no precipitate forming, fresh decalcification solution was added to the implants and the same chemical test was performed 24 hours later. Two successful tests in a row resulted in complete decalcification of the samples.

Decalcified samples were frozen in optimal cutting temperature (OCT) fluid and cut in half using a surgical blade to section the middle of the implants and the ends near the insertion points. Each region of interest was sectioned at 15 µm using a cryotome and sections were placed on charged microscope slides. Verhoeff-Van Gieson (VVG) stain was used to highlight any elastic fibers present in newly formed blood vessels. Collagen would be stained red, cells would be stained blue, elastin would be stained black, and other tissue would be stained yellow. For the VVG stain, Weigert's iodine solution was prepared by dissolving 0.2g of potassium iodide in 400 µL of distilled water. Once dissolved, 0.1g of iodine was added and allowed to dissolve. Once the iodine was dissolved, 9.6 mL of distilled water was added to dilute the solution. 10% aqueous ferric chloride was prepared by dissolving 1g of ferric chloride in 10 mL of distilled water. Verhoeff's working solution was prepared by combining 5 mL of 5% alcoholic hematoxylin, 2 mL of 10% aqueous ferric chloride, and 2 mL of Weigert's iodine solution. 2% aqueous ferric chloride was prepared by diluting 1 mL of the previously made 10% ferric chloride in 5 mL of distilled water. Van Gieson's counterstain was made by mixing 0.5 mL of 1% aqueous acid fuchsin with 10 mL of saturated aqueous picric acid.

Slides were brought to room temperature and hydrated in distilled water. Verhoeff's working solution was then applied to the sections for 1 hour. After 2-3 changes of tap water, sections were differentiated in 2% ferric chloride for 1-2 minutes. Differentiation was stopped with several changes of tap water. Slides were then treated with 5% aqueous sodium thiosulfate for 1 minute and subsequently washed in running tap water for 5 minutes. Van Gieson's solution was used to counterstain the samples for 3-5 minutes before the slides were quickly dehydrated through 95% alcohol and 2 changes of 100% alcohol. Slides were finally cleared in 2 changes of xylene for 3 minutes each. Resinous mounting medium was applied and a coverslip was placed on top of the slides.

2.1.13. Statistical Analysis

All quantitative data was subjected to a paired Student's T Test. KaleidaGraph Synergy Software was used for statistical analysis.

2.2. Results

2.2.1. Radiographic Images

The x ray images obtained at 4 and 8 weeks post-op show stable implants in both the experimental and control groups. At 4 weeks, although there is obstruction from the cast, both groups appear to be stable with no damage to the implants or the surrounding tissue. Signs of remodeling are evident at each end of the implant site and there appears to be callus formation next to the adjacent ulna in the allograft group. At 8 weeks both groups remained intact as well as the surrounding structures. Signs of remodeling and calcification are more evident at each end of the implant site in both groups and callus formation appears to be on both adjacent ulnas.

Figure 8. X ray images of the scaffold at 4 weeks post-op (A) and 8 weeks post-op (B). X ray images of the allograft at 4 weeks post-op (C) and 8 weeks post-op (D). Signs of remodeling can be seen at each end of the implant and along the nearest part of the ulna in both groups (*). Implants from both groups were intact and secured at the implant site throughout the study. The arrows indicate the location of the implants through the obstruction of the cast at 4 weeks post-op.

2.2.2. Micro CT

Micro CT analysis of the harvested implants showed a considerable amount of bone growth into and around the implants. Remodeling has occurred at each end of the implant site and on the adjacent ulna. Due to the density of the allografts, it is difficult to determine the amount of new bone growth that is taking place inside the allografts themselves. A large portion of the developing new bone seems to be at each end of the implant site and next to the adjacent ulna.

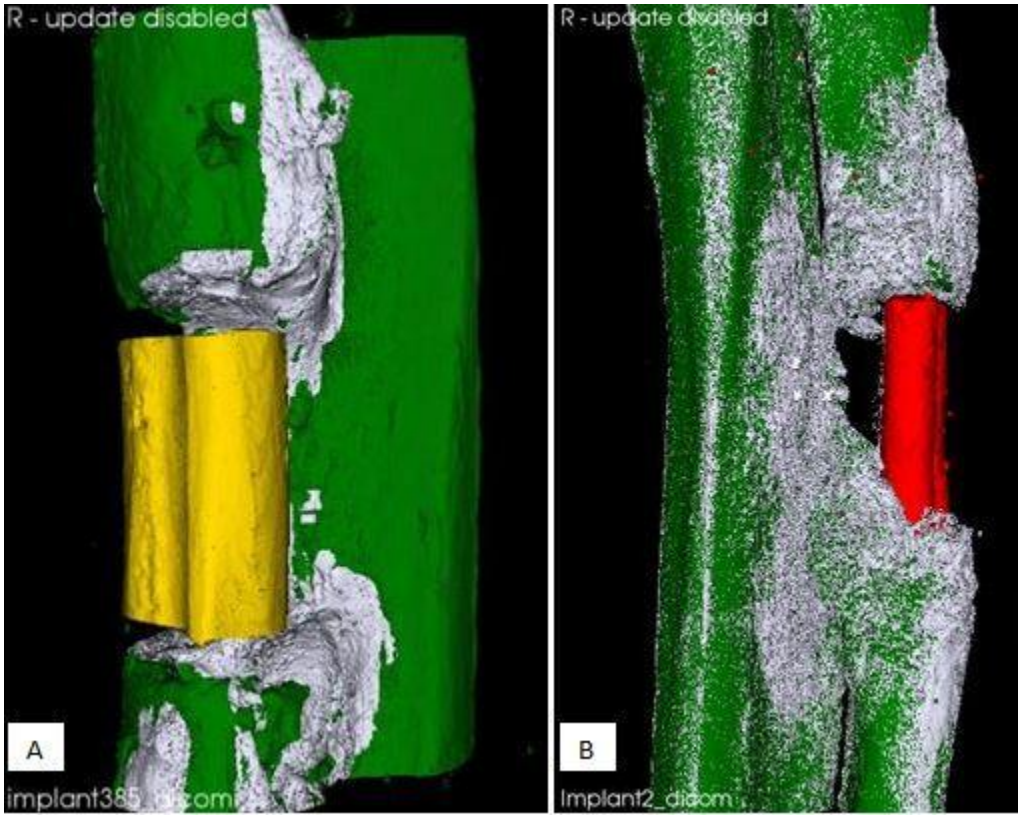

Figure 9. Micro CT images of a harvested allograft (A) and scaffold (B). Old native bone is highlighted green, new bone is highlighted lavender, the allograft is highlighted yellow, and the HAp posts are highlighted red. There is a large amount of bone growth at each end of the implant site and with the adjacent ulna in both groups. Bone is also seen growing into and around the scaffold.

Utilizing the differences in attenuation between old bone and new developing bone, the total volume of new bone that developed in each sample was quantified. The average volume of new bone in the scaffolds was 68.27 (±38.55) mm^3 while the average volume of new bone in the allografts was 76.40 (±51.38) mm^3. Although the allografts had slightly higher bone growth than the scaffolds, there is no statistical significance between the two groups (t=0.71).

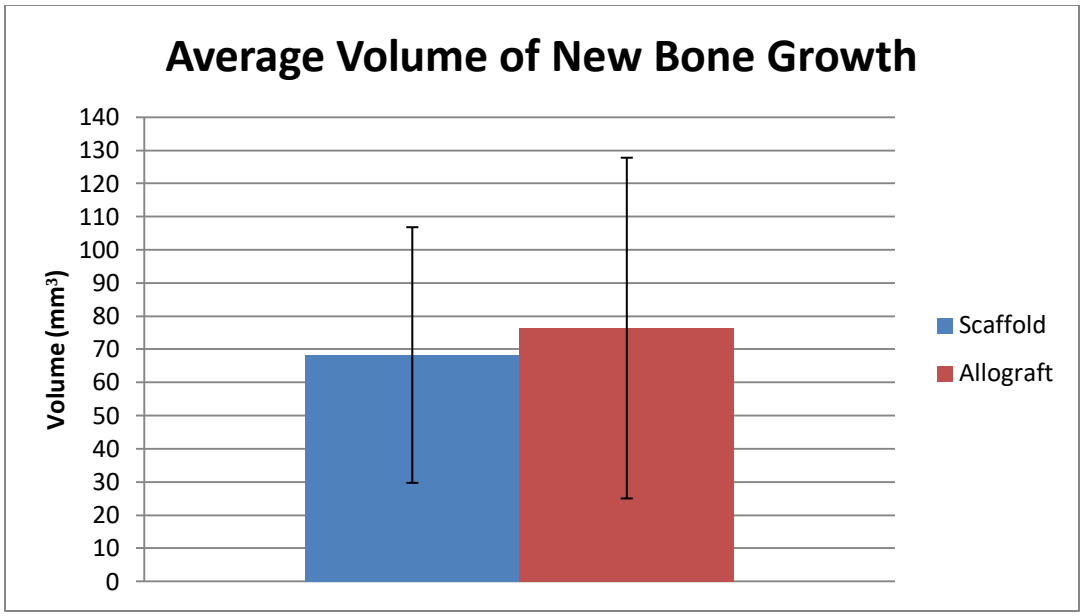

Figure 10. Average volume of new bone growth in the scaffold and allograft groups. The scaffolds had an average growth of 68.27 (±38.55) mm^3 while the allografts had an average growth of 76.40 (±51.38) mm^3 (n=4).

2.2.3. Mechanical Testing

Compressive forces were recorded by the Instron 5869 throughout the duration of the mechanical push-out test. Force was applied axially onto the scaffolds until they were visibly dislodged from the implant site or the recorded force-displacement curve dropped significantly. The ultimate push-out stress was calculated by dividing the ultimate force for each sample by the cross-sectional area. The average push-out stress for the scaffolds was 0.783 (±0.491) MPa while the average push-out stress for the allografts was 2.044 (±1.584) MPa. Despite the higher stress required to remove the allografts from the implant site, it was not statistically significant when compared to the scaffolds (t=0.28).

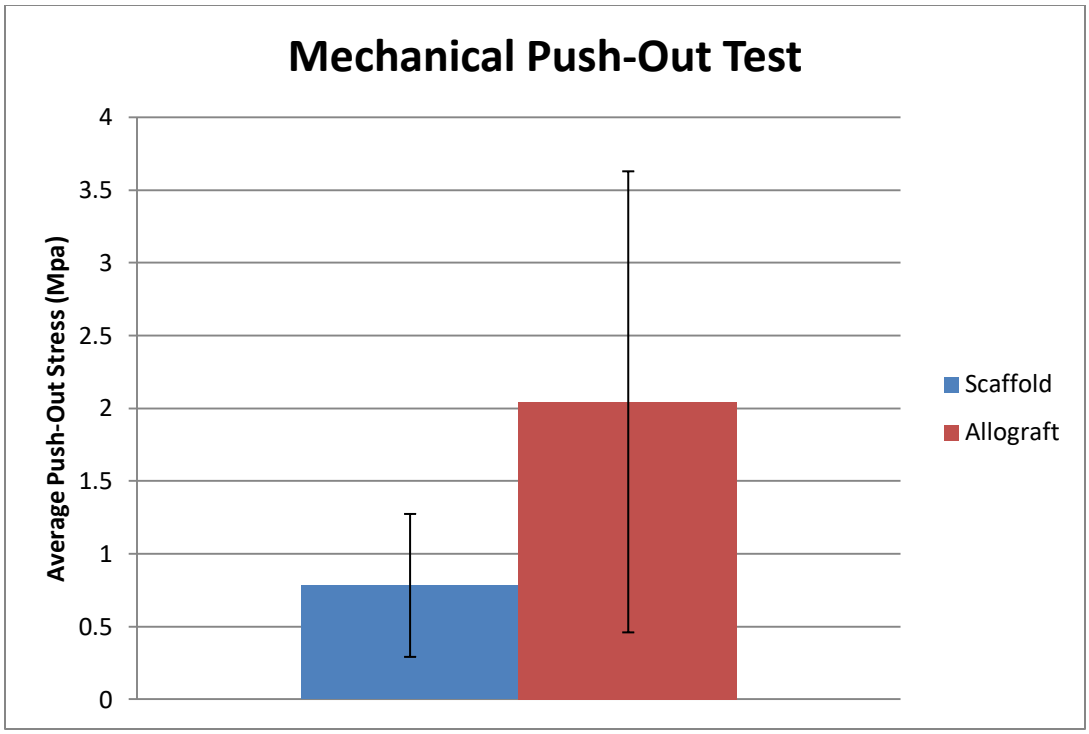

Figure 11. Average push-out stress for the scaffold (blue) and allograft (red) groups (n=4). The large standard deviation of the allograft group did not allow for a statistically significant difference between the groups.

2.2.4. Histology

Histological images of sections stained with VVG stain were obtained using a light microscope. Allografts sectioned closer to insertion points showed a considerable amount of remodeling taking place. This was evident by the number of holes and areas of apparent new collagen present in the images. Allografts sectioned from the middle of the implant stained much more intensely for collagen and there seemed to be considerably less remodeling than at the ends. Scaffolds sectioned at the ends also showed remodeling occurring in the scaffolds and the adjacent ulna. There is also evidence of collagen deposition and integration between the implants and the surrounding native bone. Scaffolds sectioned in the middle of the implant showed remodeling as well as collagen deposition within the scaffold. There is also evidence of revitalization of the

prevascularized lumens throughout some parts of the scaffold. However, it is difficult to tell whether or not any new blood vessels began to develop.

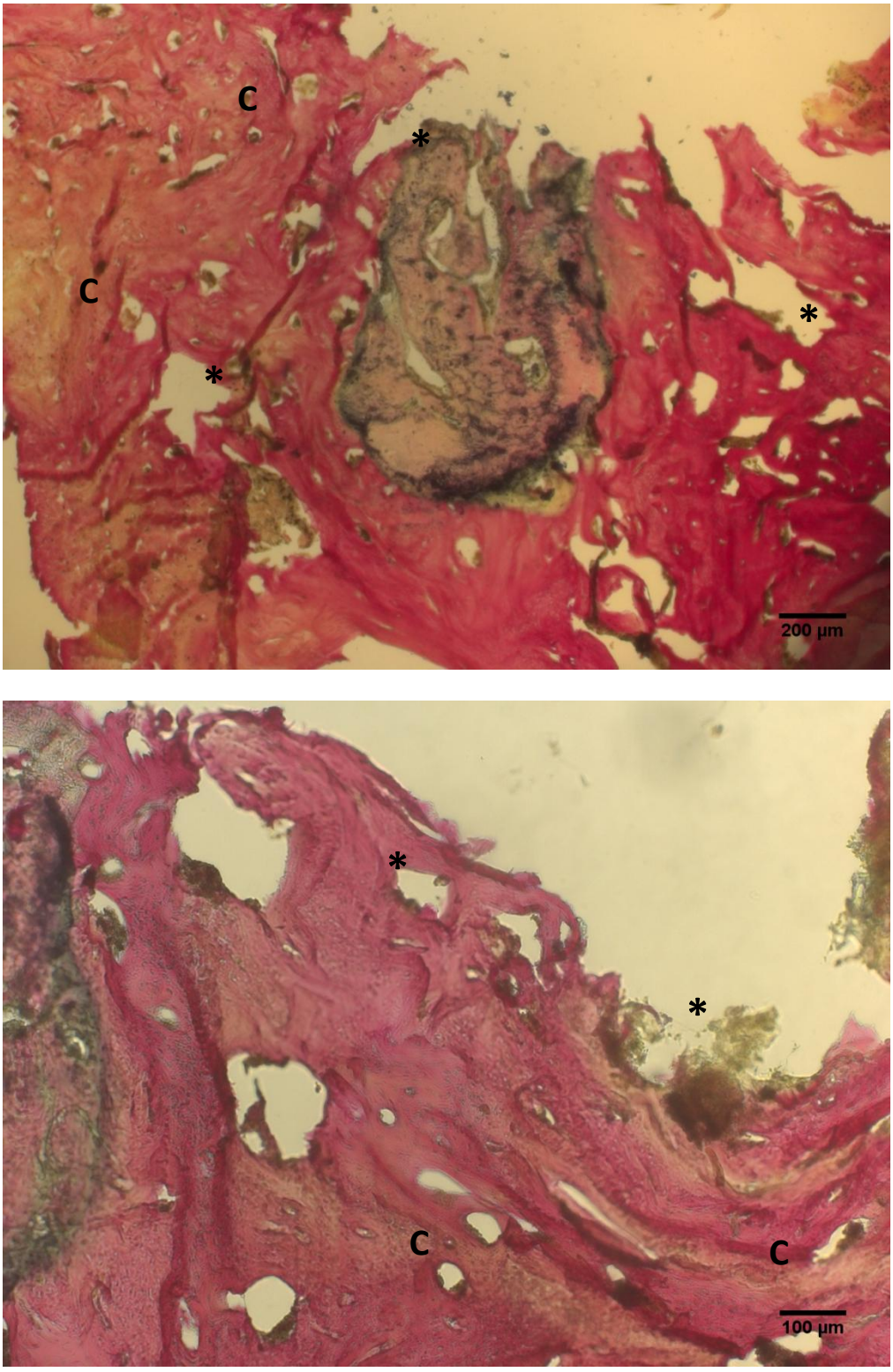

Figure 12. Histological images of the allograft sectioned at the end near the insertion point. There is a large amount of potential remodeling occurring based on the large gaps present in the collagen (*) and the deposition of new collagen (C). There are also signs of vascularization (Arrow).

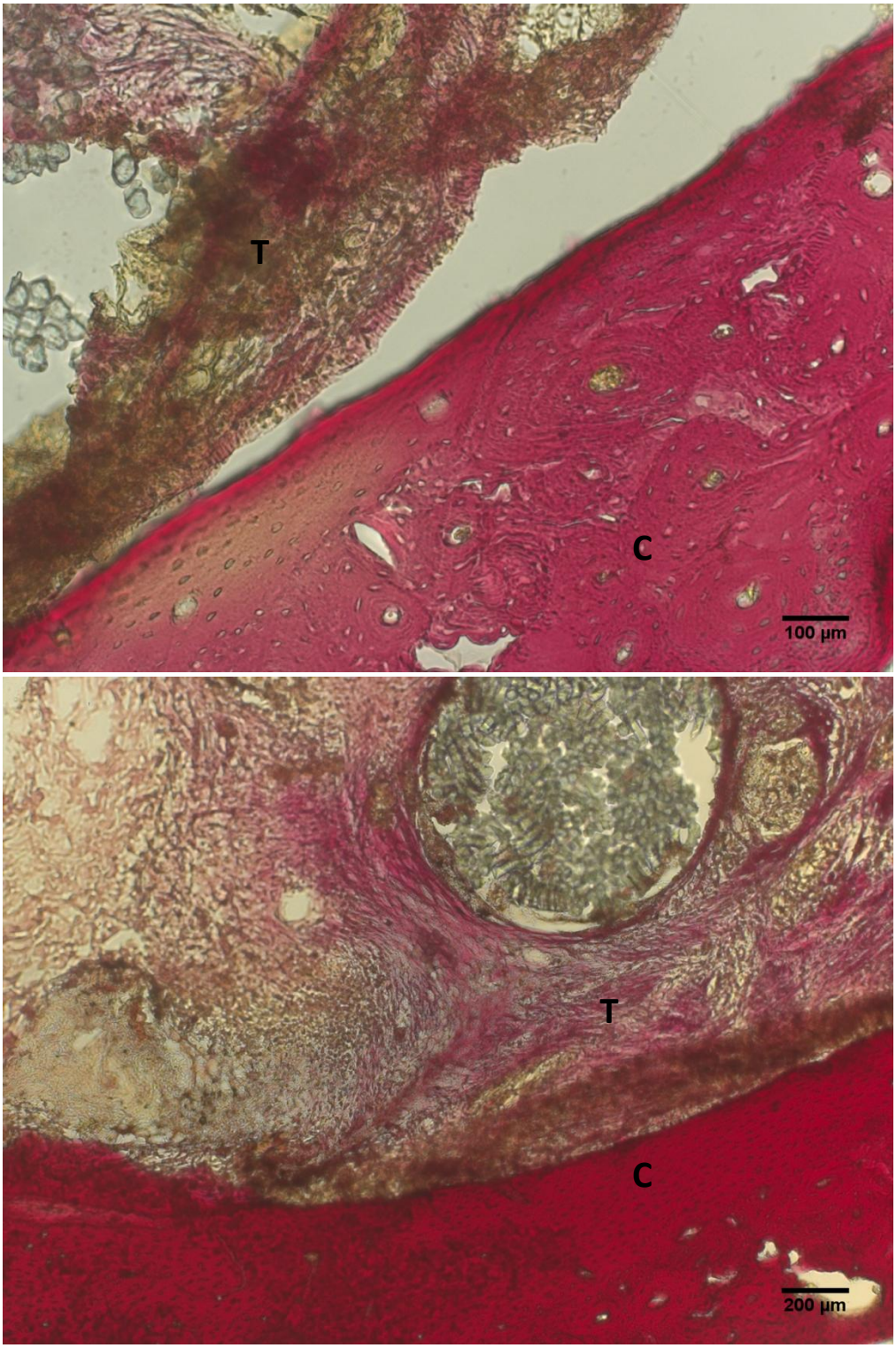

Figure 13. Histological images of the allograft sectioned in the middle. The strong staining of collagen (C) with a limited amount of deterioration or new collagen deposition indicates there was limited remodeling in the middle of the implant. The osteons (triangle) maintained their structure as well as the trabecular bone (T).

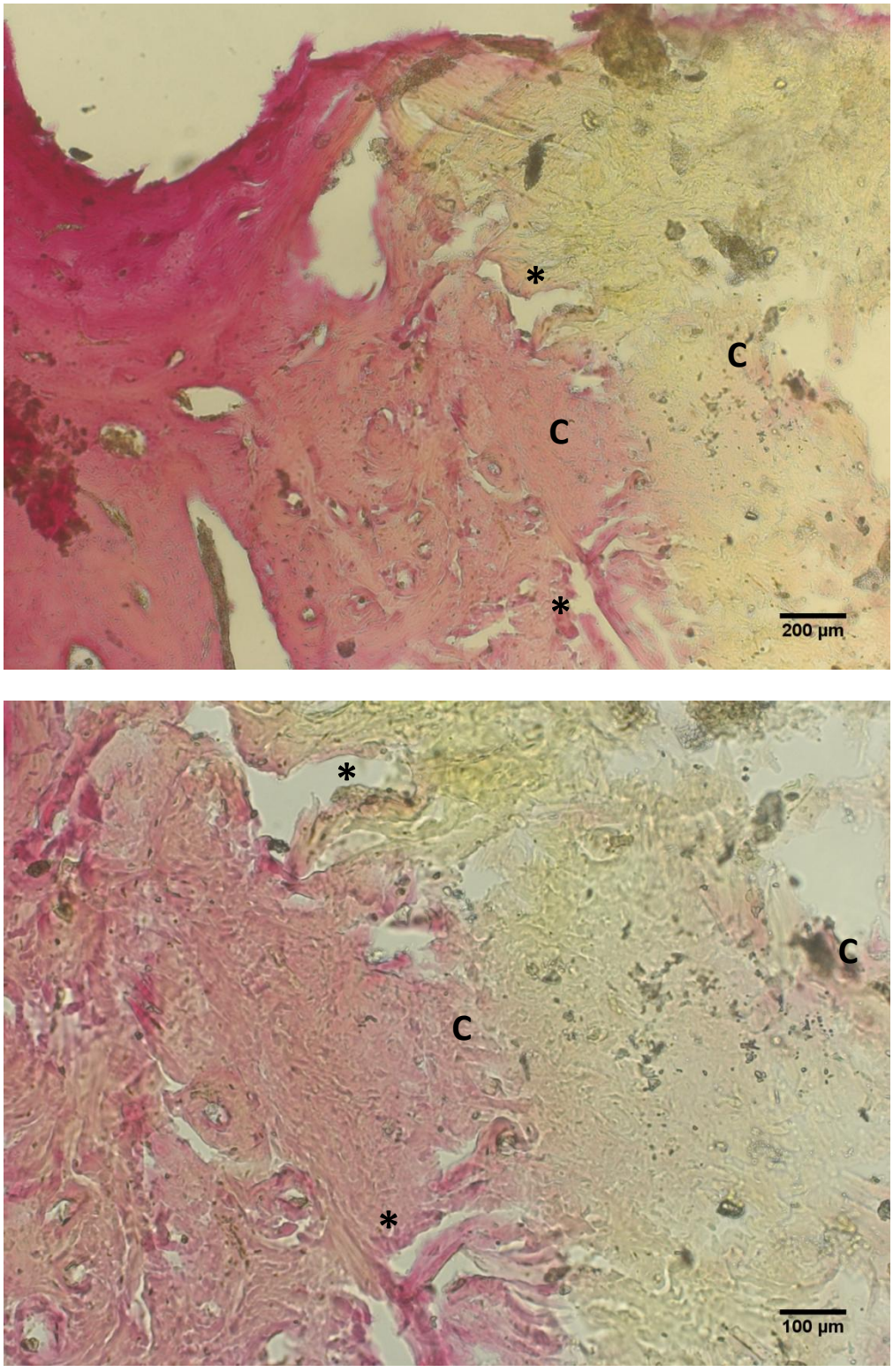

Figure 14. Histological images of the scaffold sectioned at the end near the insertion point. There is a considerable amount of remodeling occurring both in the adjacent ulna and the scaffold itself (*). The presence of collagen (C) integrating into the scaffold indicates the infiltration of surrounding cells. Collagen is also present deeper into the scaffold.

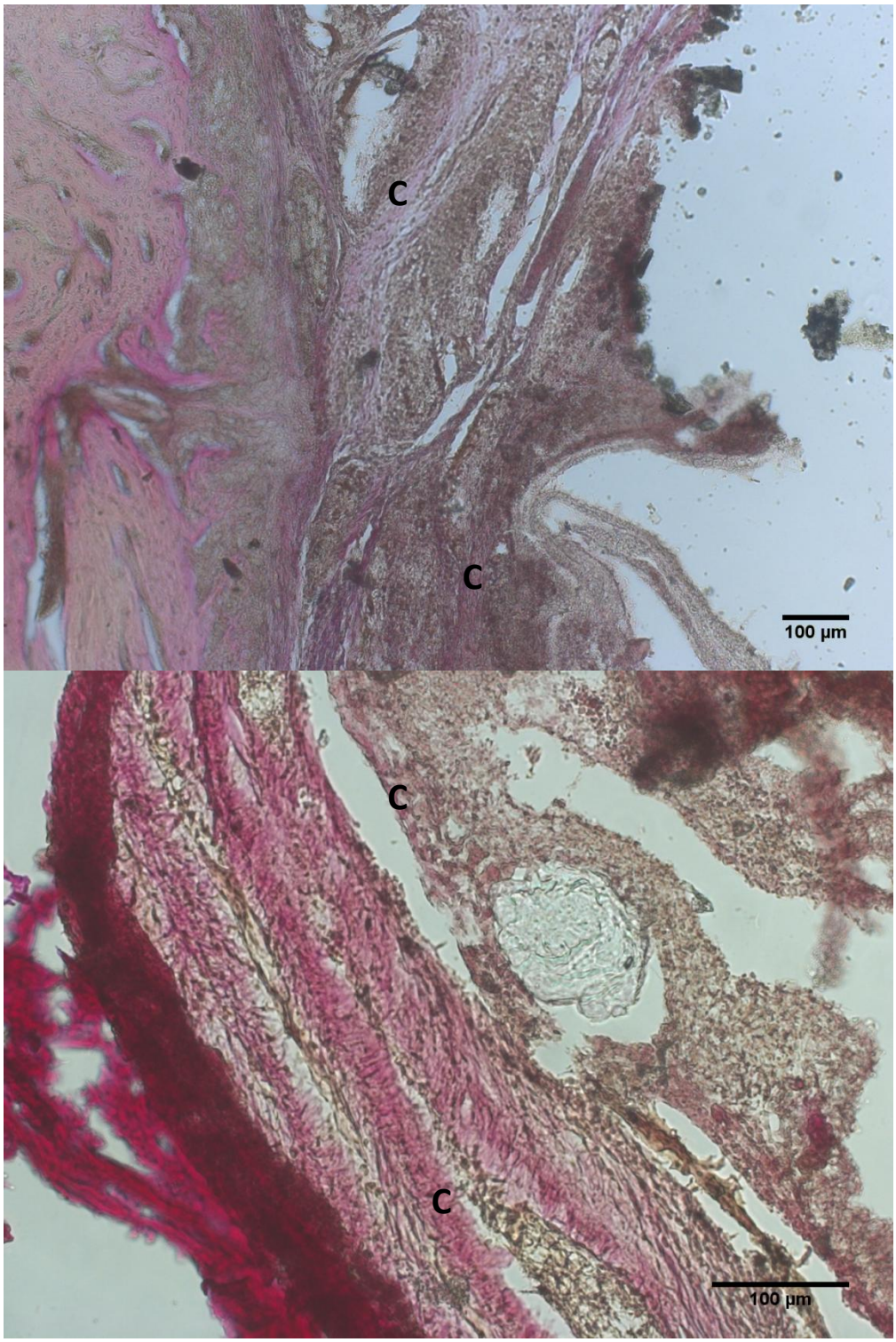

Figure 15. Histological images of the scaffold sectioned in the middle. Remodeling is occurring in the surrounding native bone as well as in parts of the scaffold itself. There is considerable collagen deposition (C) in the scaffold and tissue from the ulna seems to be integrating with the scaffold. The surrounding layer of PDLA had a large amount of collagen deposition (star) . This indicates the infiltration of cells into the scaffold from surrounding tissue. There are also signs of vascularization in various parts of the scaffold (arrow).

2.3. Discussion

The purpose of this study was to characterize a tissue-engineered scaffold for bone regeneration in a load-bearing, *in vivo* model. Scaffolds consisted of two stereoisomers of PLA (PLLA and PDLA) that were electrospun and fabricated in such a way to mimic the cortical and trabecular sections of bone. Sintered HAp columns were included in the scaffolds to provide compressive strength as well as a more biologically natural environment for cells to grow. Scaffolds were mineralized by submerging them in a SBF bath for a total of 10 hours with fresh solution added every 2 hours. 8% alginate solution was added to the cortical sections of the scaffolds prior to soaking in order to block mineralization. After mineralization, scaffolds were prevascularized by seeding HMEC-1 cells inside the cortical sections and allowing them to grow for a period of 14 days. The scaffolds were then decellularized using a freeze-thaw method which allowed for the deposited ECM to remain inside the osteons. Allografts were prepared by stripping tissue from segments of radial bone and thoroughly rinsing the trabecular section with PBS. Allografts were then sterilized using ethylene oxide gas.

A radial defect was created in adult female New Zealand white rabbits by surgically removing a piece of the radius that matched the size of the implant. The fused ulna was left intact to provide support throughout the study. 24 hours prior to implantation, scaffolds were seeded with 3-5 million rbMSCs in both the trabecular and cortical sections. Implants were secured in place with a suture and a cast was made around the surgical legs of the rabbits to provide stability for the first 4 weeks. The casts were removed after 4 weeks and the rabbits were allowed to apply normal load to the surgical leg for 4 more weeks until sacrifice.

X-ray images taken at 4 and 8 weeks post-surgery showed stable, intact implants for both the scaffold and allograft groups throughout the entire study. The surrounding anatomical structures also remained completely intact with no swelling around the surgical site. At 4 weeks there appears to be slight remodeling at each end of the implant site and some callus formation next to the adjacent ulna. At 8 weeks there is more evidence of remodeling around the implant and even more callus formation next to the ulna. There did not appear to be a noticeable difference between groups in the amount of remodeling or callus formation occurring from the x rays. It is evident that the scaffolds are able to withstand the amount of stress applied during normal load and do not entice any considerable immune reaction.

Micro CT analysis of the harvested implants allowed for visualization and quantification of the volume of new bone growth that occurred at the surgical site. The scaffold images showed a large amount of bone growth around the edges of each implant site and next to the adjacent ulna. Some samples showed new bone forming inside the scaffolds as well. The allografts mainly showed bone growth next to the adjacent ulna and at each end of the implant. Due to the density of the allografts, it was difficult to determine whether or not bone was developing inside of them. Both the scaffold and allograft groups showed a comparable quantitative volume of bone growth and there was no statistical significance between the groups. However, multiple factors may have lead to the large standard deviations seen within each group. First, one of the scaffold samples had the adjacent ulna removed after harvesting and one of the HAp columns was subsequently damaged in the process. This automatically diminished the amount of new bone that was detected during the micro CT process. Second, the preparation of the

samples after harvest may have altered the density and surface of the surrounding bone. Due to excessive scraping with a surgical blade to remove fibrous tissue, the native radius and ulna may have been scratched. This is apparent in the image of one of the samples that has a large number of divots and marks along the bone and an unusual pattern of new bone growth. Despite these discrepancies, the scaffold group shows its ability to promote bone growth into and around the implant at the same level as an allograft.

Mechanical studies were performed to measure the amount of force needed to remove the implant from the surgical site; thus indirectly measuring the amount of fusion with the surrounding native bone. A metal bar was custom made to generally match the radius of the scaffolds and allografts and was secured in place using pneumatic grips on an Instron 5869. The implants were secured in place with bench-top vises and the metal bar was used to apply an axial force onto the implant at a rate of 1 mm/min. Force was applied until the implant failed or the force-displacement curve dropped substantially. The allograft group had a higher average ultimate push-out stress when compared to the scaffold group but both values were comparable. There was a high standard deviation that did not allow for any statistical significance between groups. Similar to the variations present in the micro CT data, there were many factors that lead to differences in push-out strength. First, the adjacent ulnas were left attached to the radius to avoid damaging the implants while trying to remove them. To account for this, the ulnas were cut axially at each insertion point to reduce the affect it had on mechanical strength as much as possible. Despite attempting to cut as close to the radius as possible, it was difficult to determine whether or not the ulna was completely cut. Also, the scaffold sample that had its ulna removed and was damaged during harvest had an extremely low value compared

to most of the others. This is likely due to the lack of support from the ulna and the damage done to the scaffold. One of the allograft groups had a much higher value than all other samples in the study which may have been due to insufficient cutting of the ulna. If this value is removed from the data, the average between the two groups is much more similar (1.28 MPa for the allografts and 0.78 MPa for the scaffolds). Regardless of these discrepancies, the mechanical stress needed to remove the implants from the surgical site was comparable between both groups.

Histology using the VVG stain was performed to assess any differences between the scaffold and allograft groups. The sections taken from the ends of each group showed remodeling occurring in the implants themselves and the adjacent ulna. New collagen formation occurred for both groups and the scaffold showed integration with the surrounding native bone. When sections were taken from the middle of the implants, the allograft seemed to have much less remodeling occurring than the scaffolds. The allografts stained a dark red with less signs of new collagen formation which indicates less remodeling and infiltration of surrounding cells. The scaffolds showed clear signs of integration with surrounding bone and new collagen deposition. The PDLA layer used to secure the scaffold had collagen deposited throughout and collagen was present in the inner portions of the scaffold as well. There are also signs of revitalization of the prevascularized lumens throughout the scaffolds. However, it was difficult to obtain clean sections of the scaffolds due to the differences in modulus of the various tissues and polymers in the sample. Many of the osteons seemed to have collapsed during sectioning of the scaffolds and it was difficult to fully visualize what was being stained. Also, with a higher number of rbMSCs seeded prior to implantation there may have been considerably

more collagen deposition and vascular development throughout. Despite these problems, these results show the ability of the scaffold to promote bone growth and potentially allow for vascularization.

Chapter 3 – Conclusions and Future Directions

The tissue-engineered bone scaffold that was evaluated in this study successfully showed its comparability with an allograft. The structural integrity of the implant was not damaged throughout the 8-week, load-bearing *in vivo* study and it was not rejected by the animal. The amount of new bone growth and the mechanical properties of the scaffolds and allografts were comparable as well. These data show the viability of our scaffold as a reproducible and marketable alternative to many of today's current treatments for bone fractures.

Before making it to the market, however, more work must be done to the scaffolds. The current manufacturing techniques, such as electrospinning and compacting HAp powder, tend to be difficult to reproduce and time consuming. Our lab is in the midst of developing a method to 3D print the scaffolds that will eventually include the ceramic portion as well. In addition to ease of manufacturing, 3D printing will allow for enhanced customizability to the patients. The implant site can be directly modeled using various imaging techniques and the scaffolds can be printed to match the exact shape of the site. Also, the number of cells seeded on the scaffold prior to implantation can be greatly increased to promote more complete and rapid bone development and vascularization. Finally, an alternate method to promote vascularization is currently being studied in our lab. Seeding the scaffolds with endothelial cells for 2 weeks proves to be inefficient for mass production and does not allow for scaffold manipulation while the cells are alive. To circumvent this issue, we are developing an injectable ECM solution that will have a similar capacity to entice vascular differentiation of stem cells as the prevascularized lumen. Once these studies have been accomplished, the next step would

be to examine the scaffolds in a larger animal model, such as sheep. Although the scaffolds were exposed to natural loads in the rabbit model, the fused ulna withstood a significant amount of force as well. A larger animal model will test just how much force the scaffolds can actually bear *in vivo*. There is a large amount of potential with these tissue-engineered scaffolds and, with successful future studies, they can prove to be extremely useful in a clinical setting.

References

1. Soleymanha, Mehran et al. “Survey of 2582 cases of acute orthopedic trauma.” *Trauma monthly* vol. 19,4 (2014): e16215. doi:10.5812/traumamon.16215
2. Burge, R. , Dawson-Hughes, B. , Solomon, D. H., Wong, J. B., King, A. and Tosteson, A. (2007), Incidence and Economic Burden of Osteoporosis-Related Fractures in the United States, 2005–2025. J Bone Miner Res, 22: 465-475. doi:10.1359/jbmr.061113
3. Liu, Yan, et al. “Hierarchical Structures of Bone and Bioinspired Bone Tissue Engineering.” *Small*, vol. 12, no. 34, 2016, pp. 4611–4632., doi:10.1002/smll.201600626
4. Rodan, Gideon A. “Introduction to Bone Biology.” *Bone*, vol. 13, 1992, doi:10.1016/s8756-3282(09)80003-3.
5. Marsell, Richard, and Thomas A Einhorn. “The biology of fracture healing.” *Injury* vol. 42,6 (2011): 551-5. doi:10.1016/j.injury.2011.03.031
6. Mathew, George, and Beate P Hanson. “Global burden of trauma: Need for effective fracture therapies.” *Indian journal of orthopaedics* vol. 43,2 (2009): 111-6. doi:10.4103/0019-5413.50843
7. Brinker, Mark R., and Daniel P. O’connor. “The Incidence of Fractures and Dislocations Referred for Orthopaedic Services in a Capitated Population.” *The Journal of Bone & Joint Surgery*, vol. 86, no. 2, 2004, pp. 290–297., doi:10.2106/00004623-200402000-00011.
8. Baldwin, Paul, et al. “Autograft, Allograft, and Bone Graft Substitutes.” *Journal of Orthopaedic Trauma*, 2019, p. 1., doi:10.1097/bot.0000000000001420.
9. Long, William G. De, et al. “Bone Grafts and Bone Graft Substitutes in Orthopaedic Trauma Surgery.” *The Journal of Bone and Joint Surgery-American Volume*, vol. 89, no. 3, 2007, pp. 649–658., doi:10.2106/00004623-200703000-00026.
10. Dorozhkin, Sergey V. “Bioceramics of Calcium Orthophosphates.” *Biomaterials*, vol. 31, no. 7, 2010, pp. 1465–1485., doi:10.1016/j.biomaterials.2009.11.050.
11. Keating, J. F., and M. M. Mcqueen. “Substitutes For Autologous Bone Graft In Orthopaedic Trauma.” *The Journal of Bone and Joint Surgery*, vol. 83, no. 1, 2001, pp.-38., doi:10.1302/0301-620x.83b1.11952.
12. Howard, Daniel et al. “Tissue engineering: strategies, stem cells and scaffolds.” *Journal of anatomy* vol. 213,1 (2008): 66-72. doi:10.1111/j.1469-7580.2008.00878.x
13. Shafiee, Ashkan, and Anthony Atala. “Tissue Engineering: Toward a New Era of Medicine.” *Annual Review of Medicine*, vol. 68, no. 1, 2017, pp. 29–40., doi:10.1146/annurev-med-102715-092331.
14. Hamilton, N. J., Kanani, M. , Roebuck, D. J., Hewitt, R. J., Cetto, R. , Culme-Seymour, E. J., Toll, E. , Bates, A. J., Comerford, A. P., McLaren, C. A., Butler, C. R., Crowley, C. , McIntyre, D. , Sebire, N. J., Janes, S. M., O'Callaghan, C. , Mason, C. , De Coppi, P. , Lowdell, M. W., Elliott, M. J. and Birchall, M. A. (2015), Tissue-Engineered Tracheal Replacement in a Child: A 4-Year Follow-Up Study. American Journal of Transplantation, 15: 2750-2757. doi:10.1111/ajt.13318
15. Centanni, John M., et al. “StrataGraft Skin Substitute Is Well-Tolerated and Is Not Acutely Immunogenic in Patients With Traumatic Wounds.” *Annals of Surgery*, vol. 253, no. 4, 2011, pp. 672–683., doi:10.1097/sla.0b013e318210f3bd.

16. Jun, Indong et al. “Electrospun Fibrous Scaffolds for Tissue Engineering: Viewpoints on Architecture and Fabrication.” *International journal of molecular sciences* vol. 19,3 745. 6 Mar. 2018, doi:10.3390/ijms19030745
17. Amini, Ami R et al. “Bone tissue engineering: recent advances and challenges.” *Critical reviews in biomedical engineering* vol. 40,5 (2012): 363-408.
18. Guda, Teja, et al. “In Vivo Performance of Bilayer Hydroxyapatite Scaffolds for Bone Tissue Regeneration in the Rabbit Radius.” *Journal of Materials Science: Materials in Medicine*, vol. 22, no. 3, 2011, pp. 647–656., doi:10.1007/s10856-011-4241-7.
19. Chu, Tien-Min G., et al. “Segmental Bone Regeneration Using a Load-Bearing Biodegradable Carrier of Bone Morphogenetic Protein-2.” *Biomaterials*, vol. 28, no. 3, 2007, pp. 459–467., doi:10.1016/j.biomaterials.2006.09.004.
20. Cláudia L. S. De Oliveira Mori, et al. “Nanostructured Polylactic Acid/Candeia Essential Oil Mats Obtained by Electrospinning.” *Journal of Nanomaterials*, vol. 2015, 2015, pp. 1–9., doi:10.1155/2015/439253.
21. Barabaschi, Giada D. G., et al. “Engineering Pre-Vascularized Scaffolds for Bone Regeneration.” *Engineering Mineralized and Load Bearing Tissues Advances in Experimental Medicine and Biology*, 2015, pp. 79–94., doi:10.1007/978-3-319-22345-2_5.
22. Rezvani, Zahra, et al. “A Bird's Eye View on the Use of Electrospun Nanofibrous Scaffolds for Bone Tissue Engineering: Current State-of-the-Art, Emerging Directions and Future Trends.” *Nanomedicine: Nanotechnology, Biology and Medicine*, vol. 12, no. 7, 2016, pp. 2181–2200., doi:10.1016/j.nano.2016.05.014.
23. Taylor, Brittany L., et al. “Investigating Processing Techniques for Bovine Gelatin Electrospun Scaffolds for Bone Tissue Regeneration.” *Journal of Biomedical Materials Research Part B: Applied Biomaterials*, vol. 105, no. 5, 2016, pp. 1131–1140., doi:10.1002/jbm.b.33622.
24. Patel, Pushpendra P., et al. “Mechanical and Biological Evaluation of a Hydroxyapatite-Reinforced Scaffold for Bone Regeneration.” *Journal of Biomedical Materials Research Part A*, vol. 107, no. 4, 2019, pp. 732–741., doi:10.1002/jbm.a.36588.
25. Cipriano, James. Characterization of a pre-vascularized biomimetic tissue engineered scaffold for bone.Retrieved from https://doi.org/doi:10.7282/T35H7KQX
26. Xing, Qi, et al. “Decellularization of Fibroblast Cell Sheets for Natural Extracellular Matrix Scaffold Preparation.” *Tissue Engineering Part C: Methods*, vol. 21, no. 1, 2015, pp. 77–87., doi:10.1089/ten.tec.2013.0666.
27. Sinibaldi, Kenneth. “Harvesting, Storage, and Application of Cortical Allografts.” *Current Techniques in Small Animal Surgery*, by M. Joseph. Bojrab, Teton New Media, 2014, pp. 864–865.